CZECH TECHNICAL UNIVERSITY IN PRAGUE

FACULTY OF MECHANICAL ENGINEERING

Department of Process Engineering

Bachelor Thesis

2021

Qais Anz

CZECH TECHNICAL UNIVERSITY IN PRAGUE FACULTY OF MECHANICAL ENGINEERING

Department of Process Engineering

CFD Analysis of Feed Pellets in a Fish Farming Tank

Written by: Qais Anz

Study Branch: Mechanical Engineering

Study Program: Process Engineering

Supervisor: doc. Ing. Karel Petera, Ph.D.

BACHELOR'S THESIS ASSIGNMENT

I. Personal and study details

Student's name: **Anz Qais Elia Hanna** Personal ID number: **453674**

Faculty / Institute: **Faculty of Mechanical Engineering**

Department / Institute: **Department of Process Engineering**

Study program: **Bachelor of Mechanical Engineering**

Branch of study: **Power and Process Technology**

II. Bachelor's thesis details

Bachelor's thesis title in English:

CFD analysis of feed pellets in fish tank

Bachelor's thesis title in Czech:

CFD analýza pelet krmiva v nádrži pro chov ryb

Guidelines:

- Make a literature research concerning CFD methods focused on moving particles in fluid.
- Identify parameters of Rosin-Rammler distribution on the basis of available experimental data for feed pellets.
- Perform CFD simulation of feed pellets in a fish tank of given geometry.
- Summarize the results and propose possible improvements in future work.

Bibliography / sources:

According to the recommendation of Thesis supervisor

Name and workplace of bachelor's thesis supervisor:

doc. Ing. Karel Petera, Ph.D., Department of Process Engineering, FME

Name and workplace of second bachelor's thesis supervisor or consultant:

Date of bachelor's thesis assignment: **21.04.2021** Deadline for bachelor thesis submission: **04.06.2021**

Assignment valid until: **19.09.2021**

doc. Ing. Karel Petera, Ph.D.	prof. Ing. Tomáš Jirout, Ph.D.	prof. Ing. Michael Valášek, DrSc.
Supervisor's signature	Head of department's signature	Dean's signature

III. Assignment receipt

The student acknowledges that the bachelor's thesis is an individual work. The student must produce his thesis without the assistance of others, with the exception of provided consultations. Within the bachelor's thesis, the author must state the names of consultants and include a list of references.

29/6/2021
Date of assignment receipt

Qais AM
Student's signature

Declaration

I hereby declare that I have completed this thesis entitled **CFD Analysis of Feed Pellets in a Fish Farming Tank** independently with consultations with my supervisor, and I have attached a full list of used references and citations.

I do not have a compelling reason against the use of the thesis within the meaning of Section 60 of Act No.121/2000 Coll., on copyright, rights related to copyright and amendments of some laws (Copyright Act).

Prague, Date: ..../...../.....

……

Student Signature

ACKNOWLEDGEMENT

I would like to express my sincere gratitude and utmost respect towards my thesis supervisor Dr. Karel Petera for his continuous support, patience, and guidance that helped me complete my thesis successfully.

I would also like to express my heartfelt appreciation to my family and friends for their great and relentless support to me throughout the years of my studies.

Table of Contents

List of Figures

List of Tables

Abstract

The purpose of the study was to investigate two feeding pellet types, and assess their mean residence time in a simulated cylindrical fish tank with baffle, by the help of computational fluid dynamics. Properties of pellets from a previous sedimentation experiment were described by the Rosin-Rammler distribution in (CFD) software ANSYS Fluent. (CFD) analysis was performed using k–ω SST turbulence model and (DPM) method where the impact of pellets on flow pattern was neglected. The pellets were introduced to the simulation by the use of group injection method. For each injected position, the mean residence time was evaluated. It was observed for both pellet types, that the smallest mean residence time was positioned at the center of the tank, and the highest (MRT) was closer to the tank's bounded wall. The basis of this study could be of use to marine biologists and aquaculturist, where a favorable injected position is categorized by the type of fish cultivated in the presented tank.

Keywords: Rosin-Rammler; CFD computational fluid dynamics; SST shear stress transport; MRT mean residence time; DPM discrete phase model

Chapter 1

Introduction

Aquaculture (farming of fish under controlled conditions) is a growing industry striving to satisfy a growing market for food, as farm-reared fresh fish is increasing in popularity and profitability. Moreover, growing public demand for a healthy, tasty, and affordable food is stimulating the prosperousness in this industry. Meanwhile, the decline in wild fish populations as a result of overharvest and water pollution has promoted the culture of farm-fish that are grown in contaminant-free waters in indoor tank systems (Helfrich L. A. et al., 2013).

These tank systems are called Recirculating Aquaculture Systems (RAS) which represents a new and unique way to farm fish. Instead of the traditional method of growing fish outdoors in open ponds and raceways, this system rears fish at high densities, in indoor tanks with a "controlled" environment. Recirculating systems filter and clean the water for recycling back through fish culture tanks (Helfrich L. A. et al., 2013).

Cultivating and feeding a wide variety of fish requires the use of commercial dry feed; in other words, feeding pellets. However, the leftover fish food may lead to eutrophication of water and worsen the aquatic environment. The most common sign of an environmental problem caused by nutrient discharges in aquaculture is the accumulation of organic sediments and changes in the benthic fauna. Therefore, how to decrease the number of uneaten food pellets is a frequently discussed topic in aquaculture (Li D. et al., 2017).

The sedimentation of feeding pellets and the accumulation of uneaten food affecting the welfare of the fish being cultivated depends on various factors besides the compositions and sizes of the feeding pellets that are being used. One of the crucial factors that contribute greatly to this issue is the geometrical properties and design of the RAS being used, in which the design of the tank, in most cases, will affect the flow pattern of the fluid and the velocity profile of the pellets being used for cultivating.

In this industry, a variety of different shapes and design properties are used for the cultivation of different types of fish. The most commonly used and widely accepted standardized designs would be the cylindrical and the rectangular tanks. In this respect, the cylindrical tanks are more preferable due to the lack of corners which allow for the flow pattern of the fluid to be almost equally distributed in comparison with the rectangular design, On the other hand, the corners of the rectangular tank would have a very low flow pattern, increasing the accumulation of sedimented uneaten food in these areas, thus affecting the cleanliness of the tank and the welfare of the cultivated fish.

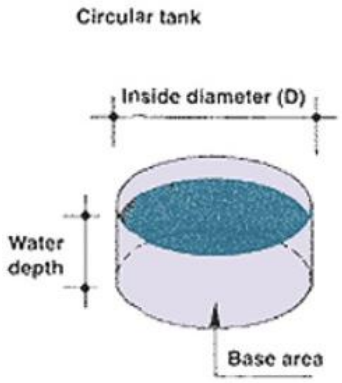

Figure 1. Representation of a circular tank

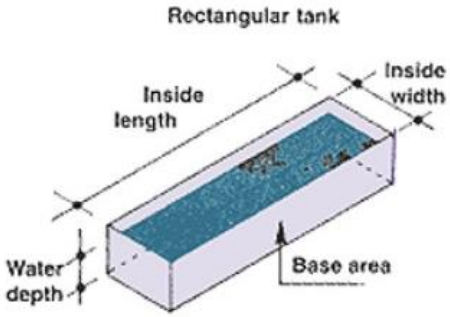

Figure 2. Representation of a rectangular tank

1.0.1 **Recirculating Aquaculture System**

Recirculating aquaculture systems (RAS) are a promising technology of fish production. They reduce aquaculture environmental impact by saving water usage via optimizing waste management and nutrient recycling. Therefore, they make intensive fish production compatible with environmental sustainability. In the meantime, water recirculation relies on the stability of physical, chemical, and biological processes to diminish the environmental impact with an optimized effluent treatment (Almeida D. B. et al., 2021).

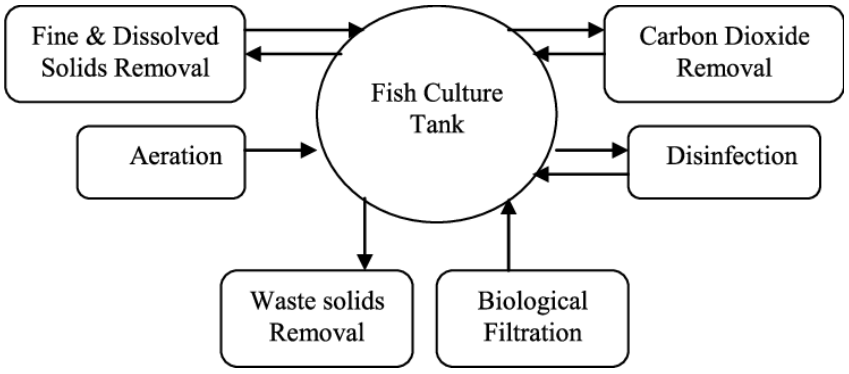

Figure 3. Work flow schematic diagram of RAS system
(Farghally H. M. et al., 2014)

1.0.2 **Benefits of Recirculating Aquaculture System**

RAS offer fish producers a variety of important advantages over open pond culture. These include a method to maximize production on a limited supply of water and land, and nearly complete environmental control to maximize fish growth year-round. The flexibility to locate production facilities near large markets helps in completing harvesting in a convenient manner, and in exercising a quick and effective disease control (Helfrich L. A. et al., 2013).

RAS can be of various sizes, ranging from large-scale production systems (over 1 million pounds per year) to intermediate-sized systems (500,000 pounds per year), to small systems (50,000 pounds per year). They can be used as grow-out systems to produce food fish or as hatcheries to produce eggs and fingerling sport fish for stocking and ornamental fish for home aquariums (Helfrich L. A. et al., 2013).

1.1 Objective and Motivation

The ever-climbing rise in human population has increased the demand for a sustainable, fresh source of fish. Broadly, people utilize detrimental methods to meet the growing demand for fish such as dynamite fishing and overharvesting rivers and lakes, which bring about calamitous effects on the environment and the ecosystem. The thesis' motive is to help the fishing sector and improve fish farming while also lowering the rate of human-caused environmental damage by implementing the use of RAS cultivating.

The main objective of this study is to look into the motion and residence time distribution of two distinct types of feeding pellets with different nutritional values in a cylindrical RAS tank. This is achieved through computational fluid dynamics (CFD) simulation and the determination of the optimal injection positions of the feeding pellets to minimize the residence time distribution (RTD) of the settling pellets, as well as maximize the expulsion of sedimented feeding pellets through the output of the tank. This reduces the accumulation of settled, uneaten food, thus decreasing bacterial growth, enhancing the water quality in the tank, and optimizing the growth rate and welfare of the fish.

Chapter 2

2.1 Computational Fluid Dynamics (CFD)

CFD codes are structured around the numerical algorithms that can tackle fluid flow problems. All commercial CFD software provide sophisticated user interfaces for inputting problem parameters and seeing the results in order to provide simple access to their computational capability. As a result, all codes have three major components: (Versteeg H. K. et al., 2007).

i. Preprocessor
ii. Solver
iii. Post processor

2.1.1 **Preprocessor**

Pre-processing is the process of entering a flow problem into a CFD program via an operator-friendly interface and then converting that input into a format that the solver can understand. It consists of several stages that can be shown below:

- Definition of the geometry in the region of interest: the computational domain
- Grid generation – the sub-division of the domain into a number of smaller, non-overlapping sub-domains: a grid (or mesh) of cells (or control volumes or elements)
- Selection of the physical and chemical phenomena that need to be modelled
- Definition of fluid properties
- Specification of appropriate boundary conditions at cells which coincide with or touch the domain boundary

2.1.2 **Solver**

There are three distinct streams of numerical solution techniques: finite difference, finite element, and spectral methods. We shall be solely concerned with the finite volume method whereas ANSYS fluent solver follows this method (Versteeg H. K. et al., 2007). the numerical algorithm consists of the following steps:

- Integration of the governing equations of fluid flow over all the (finite) control volumes of the domain
- Discretization – conversion of the resulting integral equations into a system of algebraic equations
- Solution of the algebraic equations by an iterative method

2.1.3 **Post Processor**

The post processing introduces graphical capabilities to explain and present results. These versatile data visualization tools include:

- Domain geometry and grid display
- Vector plots
- Line and shaded contour plots
- 2D and 3D surface plots
- Particle tracking
- View manipulation
- Color postscript output

2.2 Governing Equations

Computational fluid dynamics (CFD) is based mainly on fluid dynamics' governing equations. They are mathematical expressions of physics' conservation laws. The continuity, momentum, and energy equations are mathematical expressions of three fundamental physical concepts that underpin all aspects of fluid dynamics:

- Mass is conserved for the fluid
- Newton's second law, the rate of change of momentum equals the sum of forces acting on the fluid
- Energy is conserved: the rate of change of energy is equal to the sum of the rate of heat addition to and the rate of work done on a fluid particle (first law of thermodynamics)

2.2.1 Continuity equation

The fundamental physics of continuity equations is the principle of conservation of mass. Where the rate of increase of mass in a fluid element is equal to the net rate of flow mass into the fluid element, the continuity equation in conservation form could be seen in the relation below:

$$\frac{\partial \rho}{\partial t} + \nabla \cdot (\rho \vec{u}) = 0 \tag{2.1}$$

Where $\vec{u}$ is the flow velocity at a point and ρ is the density of the fluid. The first component denotes the rate of change in density over time, whereas the second denotes the net flow of mass across boundaries. For incompressible flows Eq. (2.1) can be written as:

$$\nabla \cdot \vec{u} = 0 \tag{2.2}$$

2.2.2 **Momentum conservation**

Newton's second law states that the rate of change of momentum of a fluid particle equals the sum of the forces on the particle. The Conservation of Momentum which can be referred to as the Navier-Stokes Equation is given by the relation shown below:

$$\overbrace{\frac{\partial}{\partial_t}(\rho\vec{v})}^{I} + \overbrace{\nabla\cdot(\rho\vec{v}\vec{v})}^{II} = \overbrace{-\nabla p}^{III} + \overbrace{\nabla\cdot\left(\vec{\vec{\tau}}\right)}^{IV} + \overbrace{\rho\vec{g}}^{V} \tag{2.3}$$

where p is static pressure, $\vec{\vec{\tau}}$ is viscous stress tensor and $\rho\vec{g}$ is the gravitational force per unit volume. The roman numerals in the Eq. (2.3) denote:

I. Local change with time
II. Momentum convection
III. Surface force
IV. Diffusion term
V. Mass force

According to Stoke's hypothesis, the viscous stress tensor $\vec{\vec{\tau}}$ can be defined as follows:

$$\tau_{ij} = \mu\frac{\partial_{v_i}}{\partial_{x_j}} + \frac{\partial_{v_i}}{\partial_{x_j}} - \frac{2}{3}(\nabla\cdot\vec{v})\delta_{ij} \tag{2.4}$$

If the fluid is assumed to be incompressible with a constant viscosity, the coefficient μ is assumed to be a constant. The Navier-Stokes equation simplifies to the relation shown below:

$$\rho\frac{D\vec{v}}{Dt} = -\nabla p + \mu\nabla^2\vec{v} + \rho\vec{g} \tag{2.5}$$

2.2.3 **Conservation of energy**

Conservation of Energy is the first law of thermodynamics which states that the sum of the work and heat added to the system will result in the increase of the energy in the system, this could be illustrated the equation below:

$$dE_t = dQ + dW \tag{2.6}$$

Where dQ is the heat added to the system, dW is the work done on the system and dE_t is the increment in the total energy of the system.

The energy equation is a mathematical statement that represents the conservation of energy concept and may be expressed as follows for incompressible flows:

$$\rho c_p \left[\frac{\partial T}{\partial t} + \vec{v}\nabla\, T\right] = \lambda \nabla^2 T + \dot{q}^{(g)} + \vec{\vec{\tau}} \cdot \vec{\vec{V}} \tag{2.7}$$

Where c_p is the specific heat capacity at a constant pressure, T is absolute temperature, $\dot{q}^{(g)}$ represents the internal heat sources, $\vec{\vec{\tau}}$ is the dynamic stress tensor, and $\vec{\vec{V}}$ is the symmetrical part of the velocity gradient tensor.

For the vast majority of engineering issues, it is challenging to solve these equations analytically. However, it is possible to achieve a computer-based approximate solution to the governing equations. These equations have no general closed form solution to date. We could, however, solve these equations numerically by solving a problem at discrete locations for a specific scenario. The use of discrete points allows partial differential equations to be transformed into solvable algebraic equations. This discretization can be accomplished using a variety of approaches. The one that ANSYS fluent solver methodology follows is the finite volume approach, which is based on partitioning the computational domain into a series of controlled volumes, is a highly generic discretization scheme used in CFD analysis. Over the set of controlled volumes, the differential equations are integrated using the divergence theorem. The values at the controlled volume faces are derived, based on some assumptions regarding their variation. The set of algebraic equations resulting from the presented methodology is solved iteratively, one for each control volume.

2.3 Turbulent Flows and Related Models

All flows encountered in engineering practice, simple ones, such as two-dimensional jets, wakes, pipe flows, flat plate boundary layers, and more complicated three-dimensional ones, become unstable above a certain Reynolds number. At higher Reynolds numbers, flows are observed to become turbulent. A chaotic and random state of motion develops, in which the velocity and pressure change continuously with time, within substantial regions of flow (Versteeg H. K. et al., 2007).The Reynolds number can be defined as:

$$Re = \frac{uL}{v} = \frac{\rho uL}{\mu} \tag{2.8}$$

Where ρ is the density of the fluid , u is the flow speed , L is a characteristic linear dimension or length , μ is the dynamic viscosity of the fluid, and v is the kinematic viscosity of the fluid. The Reynolds number of a flow gives a measure of the relative importance of inertia forces and viscous forces. In experiments on fluid systems, it is observed that at values below the so-called critical Reynolds number Re_{crit}, the flow is smooth, and adjacent layers of fluid particles slide past each other in an orderly fashion. If the applied boundary conditions do not change with time, the flow is steady. This regime is called laminar flow (Versteeg H. K. et al., 2007).

At values of Reynolds number above Re_{crit} a complicated series of events takes place, which eventually leads to a radical change of the flow character. In the final state, the flow behavior is random and chaotic. The motion becomes intrinsically unsteady even with constant imposed boundary conditions. The velocity and all other flow properties vary in a random and chaotic way. This regime is called turbulent flow (Versteeg H. K. et al., 2007).

2.3.1 **Turbulent Models**

Turbulence modeling is commonly used in computational fluid dynamic simulations, whereas the majority of engineering cases involve turbulent flow. However, there is no universal turbulent model that can be used in all engineering applications. The selection of the ideal turbulent model is critical for proper recovery and work safety, whereas it is determined by the flow character. Three basic approaches to the turbulent models can be shown below:

- Reynolds Averaged Navier-Stokes (RANS)
- Direct Numerical Simulation (DNL)
- Large Eddy Simulation (LES)

2.3.2 **Reynolds Averaged Navier-Stokes (RANS)**

A detailed description of the turbulent eddies is not required in this standard practice, and a general understanding of what happens to the flow field is sufficient. The random nature of a turbulent flow precludes an economical description of the motion, for all fluid particles. The velocity in Figure 4. is decomposed into a steady mean value U with a fluctuating component $u'(t)$ superimposed on it. This relation is called Reynolds decomposition which is shown below:

$$u(t) = U + u'(t) \tag{2.9}$$

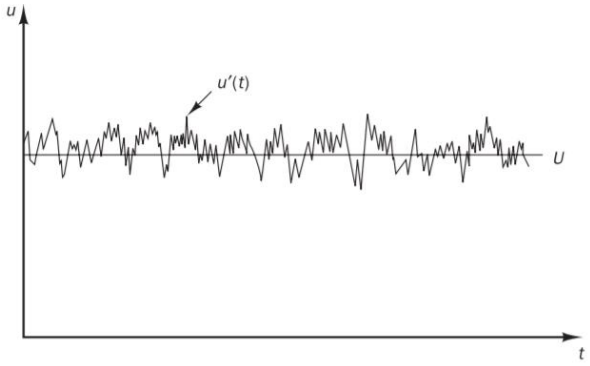

Figure 4. Typical point velocity measurement in turbulent flow
(Versteeg H. K. et al., 2007)

The Reynolds Averaged Navier-Stokes approach is a method of analyzing a turbulent flow. In engineering applications, RANS turbulence models are very frequently used due to their substantially smaller computational requirements, compared to LES or DNS approach, even though they are not generally universal, therefore some experience is necessary with these models and their validations with respect to the experimental data, which is usually necessary. In the Navier-Stokes equation, the velocity fluctuation with respect to time is separated from the mean flow velocity and pressure of fluid by averaging of the Navier-Stokes equation. The resulting equation is called Reynolds-Averaged Navier-Stokes (RANS). The RANS equation can be written in tensor notation which is shown below (White F. M., 2007).

$$\frac{\partial}{\partial t}\left(\rho\bar{u}_j\right) + \frac{\partial}{\partial x_j}\left(\rho\bar{u}_i\bar{u}_j\right) = -\frac{\partial \bar{p}}{\partial x_j} + \frac{\partial}{\partial x_j}\left(\mu\frac{\partial \bar{u}_i}{\partial x_j}\right) + \frac{\partial R_{ij}}{\partial x_j} \tag{2.10}$$

Where R_{ij} is the Reynolds stress tensor, which describes the component of the total stress tensor in a fluid, obtained from the averaging operation over Navier-Stokes equation, to account for turbulent fluctuations in fluid momentum.

Due to new unknowns introduced, such as Reynolds stress tensor and turbulent fluxes, Eq. (2.10) is not fully developed yet. Additional equations are required in order to close the system by a turbulence model.

2.4 Modeling Particle Transport

2.4.1 Lagrangian and Eulerian methods

Generally, there are two methods of modeling particle transport in computational fluid dynamic simulations, the Eulerian and the Lagrangian method.

The Eulerian method treats the particle phase as a continuum and develops its conservation equations on a control volume basis and in a similar form as that for the fluid phase. The Lagrangian method considers particles as a discrete phase and tracks the pathway of each individual particle. By studying the statistics of particle trajectories, the Lagrangian method is also able to calculate the particle concentration and other phase data. Within each kind of the particle models, there are many different models to address various characteristics of particle motion and dispersion (Zhang Z. et al., 2007).

To choose the Eulerian or the Lagrangian method for certain problem depends highly on the objective and characteristics of the problem under examination. The Eulerian method has gained its popularity on studying particle concentration distributions in indoor environments. The Lagrangian method is mainly used to predict the overall particle dispersion pattern and the temporal development of the mean concentration (Zhang Z. et al., 2007).

In the case beforehand, a case study in which mean concentration is not the primary concern, but rather overall particle dispersion pattern, in which a Lagrangian model is preferred to be implemented and used in ANSYS fluent solver.

2.4.2 **Drag of Non-Spherical Particles**

There are well over 30 equations in the literature relating the drag coefficient C_D to the Reynolds number Re of spheres falling at their terminal velocities. These correlations are of varying complexity, and contain as many as 18 arbitrary constants. However, for non-spherical particles there is no generalized expression of $C_D$vs Re available (Haider A. et al., 1989).

Nonetheless, dealing with particulate flows, researchers frequently assume particles to be perfectly spherical. This oversimplified assumption is mainly due to the fact that characterizing non-spherical particles is complex and model simplicity brings a fast computation (Yan S. et al., 2019). For spherical particles, the drag coefficient is determined by the following relation:

$$C_D = \frac{4}{3}\frac{dp(\rho_p - \rho_f)g}{u^2\rho_f} \tag{2.11}$$

Where dp is particle diameter, u the characteristic velocity, ρ_p and ρ_f are effective density of the particle and liquid phase, respectively. The drag coefficient C_D is usually expressed in terms of Reynolds number shown in the Equation. (2.8). For smooth spherical particles (Morsi S. A. et al., 1972) presented a correlation describing it, this correlation is what ANSYS fluent uses to describe the drag coefficient for smooth spherical particles. The equation could be seen below:

$$C_D = a_1 + \frac{a_2}{Re} + \frac{a_3}{Re^2} \tag{2.12}$$

For different ranges of Re, constants a_1, a_2, and a_3 are determined. The drag coefficient C_D, varies depending on particle and flow properties. Since we are dealing with particles of varying shapes, (Haider A. et al., 1989) presented the equation of drag coefficients for non-spherical particles which could be shown in the next page.

$$C_D = \frac{24}{Re}(1 + b_1 Re^{b_2}) + \frac{b_3}{1 + \frac{b_3}{Re}} \tag{2.13}$$

This relationship is reported to be valid for $Re < 2.5 \times 10^4$. Where the parameters b_1, b_2, and b_3 are defined as:

$$\begin{aligned} b_1 &= exp\,(2.3288 - 6.4581\phi + 2.4486\phi^2) \\ b_2 &= (0.0964 + 0.5565\phi) \\ b_3 &= exp\,(4.905 - 13.8944\phi + 18.4222\phi^2 - 10.2599\phi^3) \\ b_4 &= exp\,(1.4681 + 12.2584\phi - 20.7322\phi^2 + 15.8855\phi^3) \end{aligned} \tag{2.14}$$

Here ϕ is called the sphericity which was presented by (Wadell H. A., 1934), introducing the concept of particle sphericity. Their relation could be shown below:

$$\phi = \frac{s}{S} \tag{2.15}$$

Where *s* is the surface of a sphere having the same volume as the particle and *S* is the actual surface area of the particle. The sphericity, or in other words the shape factor, could not exceed the value of 1, the sphericity used for this study $\phi = 0.874$,for a cylinder with height equal to diameter. The Eq. (2.13) is used in ANSYS fluent solver to determine the drag coefficient for irregular particle shapes. In which this study used to run a computational fluid dynamics simulation on different types and shapes of fish feeding pellets.

Chapter 3

3.1 Provided Experiment and Results

3.1.1 Experiment

This study used two different pellets (particles) in terms of composition, to obtain results. The first, TM0, used fish meal, plant-based ingredients, and fish oil as protein and lipid sources. In the second, TM75, insect meal was used to replace 75 percent of the fish meal. The composition and ingredients table are shown below (Papáček Š. et al., 2020).

Table 1. Ingredients and composition of TM0 and TM75 as measured at the South Bohemia University FFPW (Papáček Š. et al., 2020).

Ingredients (g kg^{-1})	**TM0**	**TM75**
Fish meal	250	62.5
Soybean protein concentrate	120	120
Wheat gluten meal	150	150
Corn meal	100	100
Soybean meal	150	150
Wheat meal	62	54.8
Tenebrio molitor meal	0	187.5
Fish oil	80	83
Vegetable oil	60	63
Mineral supplement	10	10
Vitamin supplement	10	10
Methionin	8	9.2
Proximate Composition		
Dry matter (g $100g^{-1}$)	90.0	90.3
Crude protein (g $100g^{-1}$)	44.9	44.7
Ether extract (g $100g^{-1}$)	17.3	17.1
Ash (g $100g^{-1}$)	5.4	4.0

From each batch, twenty pellets were chosen randomly. Several pellets were introduced to a water column shown in (Figure 6.) for the purpose of measuring and recording the settling velocity of each particle.

Figure 5. Photo of feed pellets TM75

Figure 6. Illustrative image of a feed pellet settling in a water column

A camera of 29.879 fps (frames per second) was used to determine and record the particle trajectory within a water column of total height of 300 mm. The measured settling trajectory was then within the bottom part of it where it reached 224 mm, at this point constant terminal velocity could be expected and likely to occur. The settling trajectory measurement accuracy was estimated as ±0.14 mm (based on the camera resolution). The time necessary to evaluate the settling velocity was determined from the recorded movie with accuracy limited to one frame. The frame rate accuracy of the camera was estimated as 0.06% (Papáček Š. et al., 2020) (Miardi. A., 2020).

3.1.2 **Density of The Pellets**

Due to the porous characteristic of the pellet, it is possible to argue that it absorbs water during settling process, changing the density significantly. As a result, it is critical to determine the pellet's effective density in water. Assuming that the characteristic size (diameter) of the particle is known, the effective density of the particle could be calculated by the equation shown below.

$$\rho_p = \rho_f + \frac{3}{4}\frac{\rho_f C_d u^2}{g d_p} \tag{3.1}$$

Where u is the determined settling velocity of the pellets that was sedimenting in the water column. The characteristic size dp ,was based on the static camera picture with an estimated accuracy of 0.06 mm. The calculations for this experiment corresponded to a temperature of 20˚C, density $\rho_f = 998.2\ kg/m^3$ and kinematic viscosity $v = 1.004 \times 10^{-6} m^2/s$. The tables below summarize and represent, the calculated effective densities and settling velocity values, for the TM0 and TM75 feeding pellet types.

Table 2. TM0 pellets experimental results for settling velocity and effective density (Papáček Š. et al., 2020)

	Char. Size (mm)	Time (s)	Velocity (cm/s)	Re	C_d	Density (kg/m^3)
1	3.5	3.667	6.109	212.947	0.8845	1070.2
2	3.9	3.466	6.463	251.044	0.8515	1067.8
3	3.5	3.57	6.275	218.733	0.8786	1073.6
4	3.2	7.1	3.155	100.556	1.1519	1025.5
5	3.5	4.967	4.510	157.213	0.9679	1041.1
6	3.8	4.566	4.906	185.679	0.9184	1042.6
7	3.5	3.933	5.695	198.545	0.9011	1061.9
8	3.4	4.56	4.912	166.352	0.9500	1049.7
9	3.5	4.8	4.667	162.683	0.9569	1043.6
10	3.2	4	5.600	178.486	0.9293	1067.7
average	3.5	4.463	5.229	183.224	0.9390	1054.4 ± 1.1%

Table 3. TM75 pellets experimental results for settling velocity and effective density (Papáček Š. et al., 2020)

	Char. Size (mm)	Time (s)	Velocity (cm/s)	Re	C_d	Density (kg/m^3)
1	3.9	5.2	4.308	167.331	0.9482	1032.6
2	2.9	3.7	6.054	174.868	0.9351	1088.4
3	3.5	3.9	5.744	200.225	0.8990	1062.9
4	3.5	3.9	5.744	200.225	0.8990	1062.9
5	3.0	3.367	6.653	198.789	0.9008	1099.6
6	3.5	2.966	7.552	263.276	0.8434	1103.1
7	3.0	5.067	4.421	132.094	1.0302	1049.4
8	3.8	2.6	8.615	326.080	0.8148	1119.7
9	3.9	3.667	6.109	237.284	0.8619	1061.1
10	3.0	5.1	4.392	131.240	1.0328	1048.9
average	3.4	3.947	5.959	203.141	0.9165	1072.9 ± 1.9%

3.2 Pellet Diameter Measurement

The diameters of the pellets were measured using image processing in order to obtain an accurate size distribution of the pellets that will be further expanded upon in the following chapter. To ensure uniform light intensity across the sample, pellets from each group were scattered on white paper and placed in a single-layer white fabric tent. They were then photographed with a digital camera under a florescent light system. The digital camera was placed vertically 46 cm away from the sample within the tent. The photographs were taken in Nikon raw format and then transferred to a computer for further processing. All images were then processed using the MATLAB image processing toolbox. The diameters of the pellets were measured, recorded, and exported into tables, for further studying and processing (Papáček Š. et al., 2020).

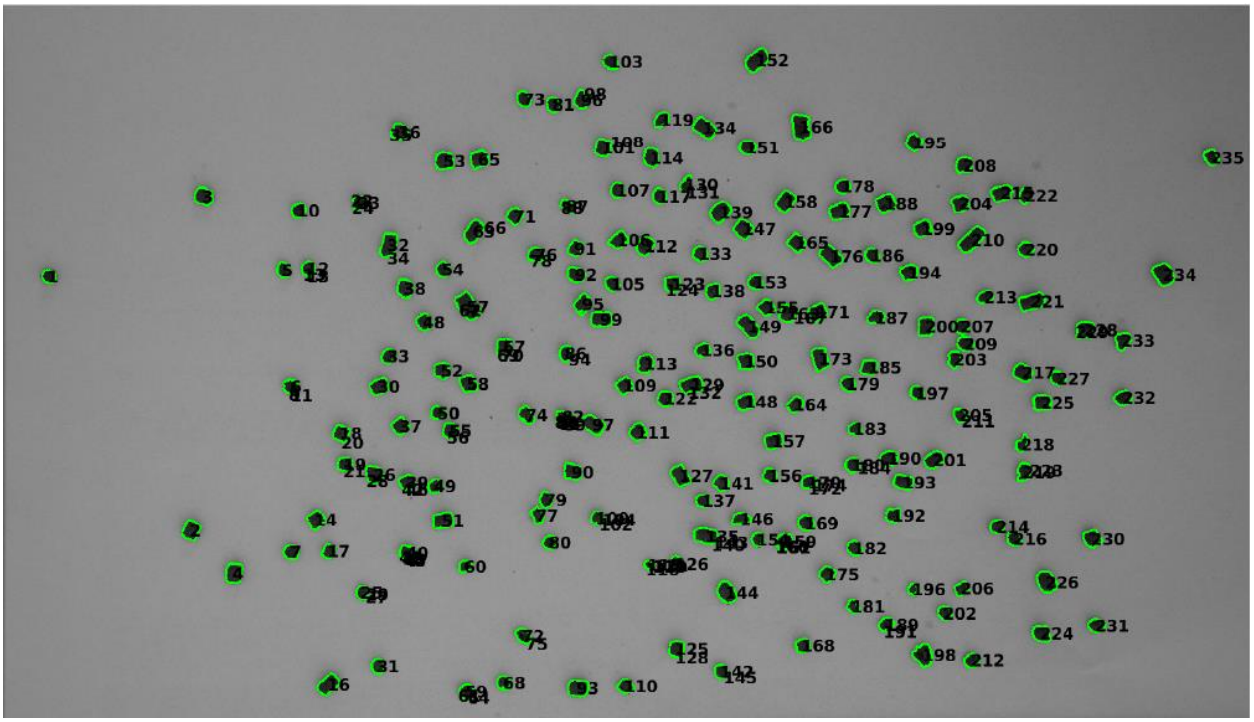

Figure 7. Measured diameter of pellets using MATLAB image processing toolbox (Papáček Š. et al., 2020)

3.2.1 **Size Distribution**

In this work, pellets of different batches and dimensions were introduced to a size distribution methodology, in which ANSYS fluent solver implements for this experiment. This method is called the Rosin-Rammler distribution, which describes the mass fraction of particles with a diameter greater than d. The relation can be described as:

$$Y_d = exp^{-(d/\bar{d})^n} \tag{3.2}$$

Where, Y_d is described as the mass fraction distribution of the function, d is the particle diameter, n is the spread parameter, and $\bar{d}$ is the mean diameter of the particle in this distribution. The data and results from the experiment provided in Figure 7. was used to find the $\bar{d}$ mean diameter and n the spread parameter, for both TM0 and TM75 feeding pellet types, where pellets with diameters below 0.5 mm were excluded, obtaining 173 points of data for the TM0 type and 350 data points for the TM75 type. The results obtained could be shown below.

For the TM0 type results are:

$$\bar{d} = 3.59\ mm \quad , \quad n = 7.56\% \tag{3.3}$$

As for the TM75 type:

$$\bar{d} = 3.27\ mm \quad , \quad n = 8.83\% \tag{3.4}$$

The data for each pellet type was then represented in a code which was written in MATLAB, using the $(nlinfit)$ function, that helps in obtaining a best fit curve in for a given data and plotting it graphically, using the MATLAB plotting tool kit. A representation of the code used and the plotted curves is shown in the next page.

```
data = load('Tm75.csv');          %  Data input for TM75 type
Xi = data(:,1); Yi = data(:,2);   %  Yi is cumulative mass % Xi diameter
mtotal = max(Yi)
Yi = 1-Yi/mtotal;  % Yi is cumulative mass fraction of diameters greater
                   % than current value on x-axis

plot(Xi,Yi,'*');
fun = @(b,x) exp( -(x/b(1)).^b(2) );
[beta] = nlinfit(Xi,Yi,fun,[3,1])
plot(Xi,Yi,'*', Xi,fun(beta,Xi),'b-');
min(Xi)
max(Xi)
grid on;
```

Figure 8. Representation of the MATLAB code used for the TM75 type

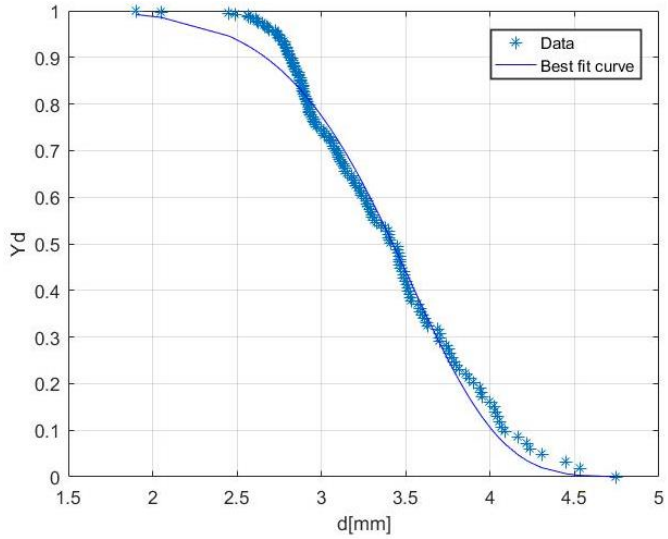

Figure 9. TM0 experimental pellet data fitted in a Rosin-Rammler distribution curve

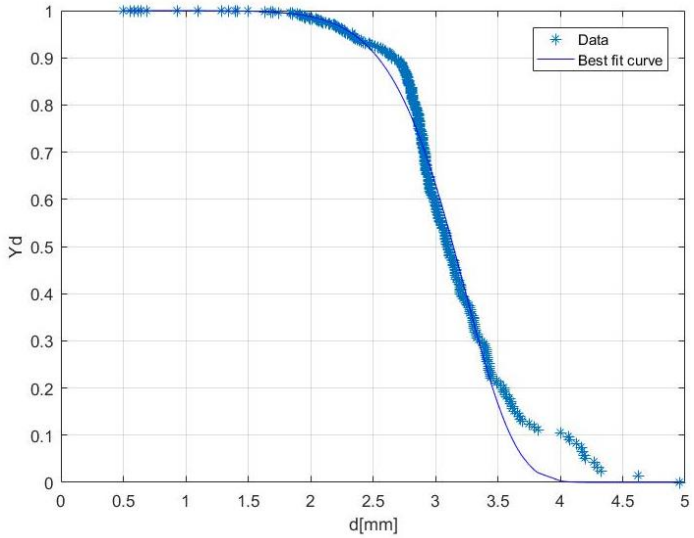

Figure 10. TM75 experimental pellet data fitted in a Rosin-Rammler distribution curve

Chapter 4

4.1 Simulated Experiment and Results

4.1.1 Tank Geometry

For any given computational fluid dynamic simulation, initial conditions prior to the analysis should be set and defined. The first condition, is setting a geometrical fluid domain model that the study will occur in, which in the case for this study, is a cylindrical tank with a baffle. A representation of the tank could be shown below. This geometry was created in ANSYS Design Modeler and provided by (Hanák J., 2016).

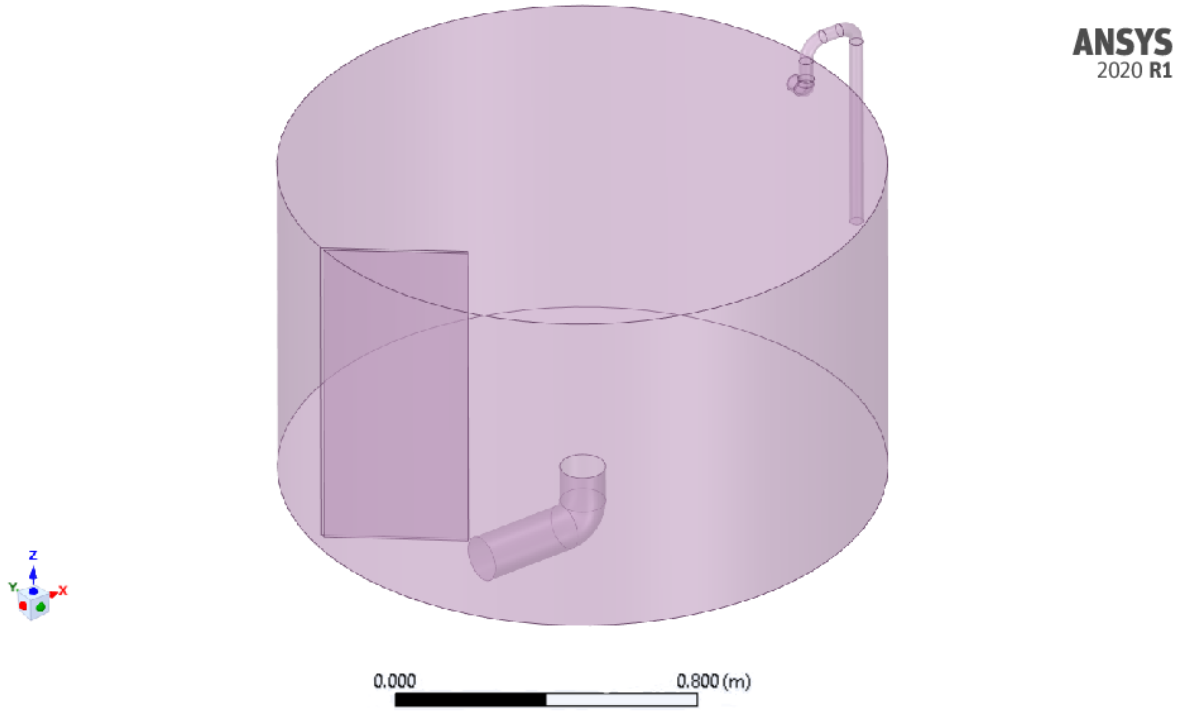

Figure 11. Geometrical model of the cylindrical tank used, generated by ANSYS CFD software package

The geometrical properties of the presented cylindrical tank in Figure 11., could be described as the following:

- Diameter of the cylindrical tank = 1465 mm
- Height of the tank = 840 mm
- Height of the inlet = 805.8 mm
- Inlet Diameter = 33 mm
- Outlet Diameter = 110 mm
- Baffle length = 840 mm
- Baffle width = 350 mm

4.1.2 **Mesh Generation and Quality**

Mesh generation is a crucial preprocessing step that is necessary to the computational simulation. It involves discretizing the domain of interest, based on the topology of the elements that fill the domain. The mesh generation process can be divided into two categories; Structured and unstructured meshes.

A structured mesh has eight nodal corner points in three dimensions and is characterized by regular connectivity. It locates neighboring cells using a Cartesian system with (i, j, k) indexing. On a regular orthogonal geometry, creating a structured mesh is the simplest technique to undertake, since a Cartesian mesh can be conveniently generated. Structured mesh generation for complex geometries on the other hand, is a time-consuming task because, based on the nature and complexity of the geometry, it may be necessary to manually break the domain into several blocks.

An unstructured mesh is a collection of elements with explicitly defined connectivity, which are typically tetrahedral, hexahedral, or polyhedral mesh elements. The unstructured mesh generation process involves two basic steps, point creation and definition of connectivity between these points. The unstructured mesh is usually a good choice, because of its adaptability and automation, though due to the presence of skewed elements in sensitive regions like boundary layers, solution accuracy may be unfavorable compared to the structured mesh.

Regardless of structured or unstructured meshes, one of the primary sources in determining a mesh quality is the cell shape, which can be characterized by its skewness and aspect ratio, where mesh skewness is determined by the angle made between gridlines, or based on the equivalent area of the actual cell (volume in 3D) relative to its equilateral cell. In this regard, ANSYS Fluent meshing quality is defined by a metric mesh spectrum, that could be summarized by the representation below.

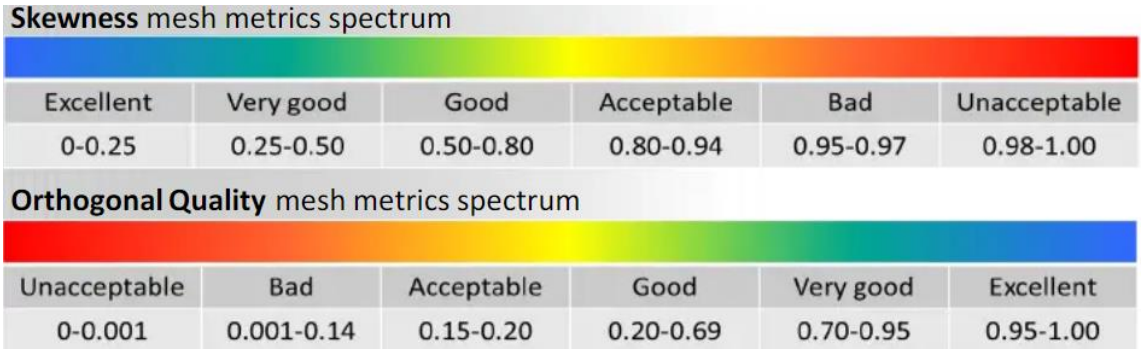

Figure 12. Metric mesh quality spectrum utilized by ANSYS (ANSYS Inc., 2015)

For this study three different types of mesh methods were used to simulate the results, for the purpose of comparing and improving the mesh quality for each given mesh type. This comparison helped in choosing a meshing method that attains the highest mesh quality for the given task. A description of the obtained comparison could be seen below.

Table 4. Mesh qualities for different meshing methods

Meshing method	Number of elements	Maximum skewness	Minimum Orthogonal Quality
Tetrahedral	826874	0.85288346	0.15
Polyhedral	228386	0.81514416	0.18
Poly-hexcore	494685	0.79985045	0.20

The mesh method that gives the best quality after the comparison, is the Poly-hexcore method which is a part of ANSYS Fluent Meshing tool, this method obtained the highest maximum skewness and minimum orthogonal quality, this means that the method will have a better accuracy and efficiency in obtaining results. The Poly-hexcore, is a relatively new (Mosaic, 2018) technology application that ANSYS adapted, This method links high quality octree-based hexahedral mesh elements in the bulk region, and isotropic poly-prisms in the boundary layer with Mosaic polyhedral elements. A representation of the mesh generated could be seen below.

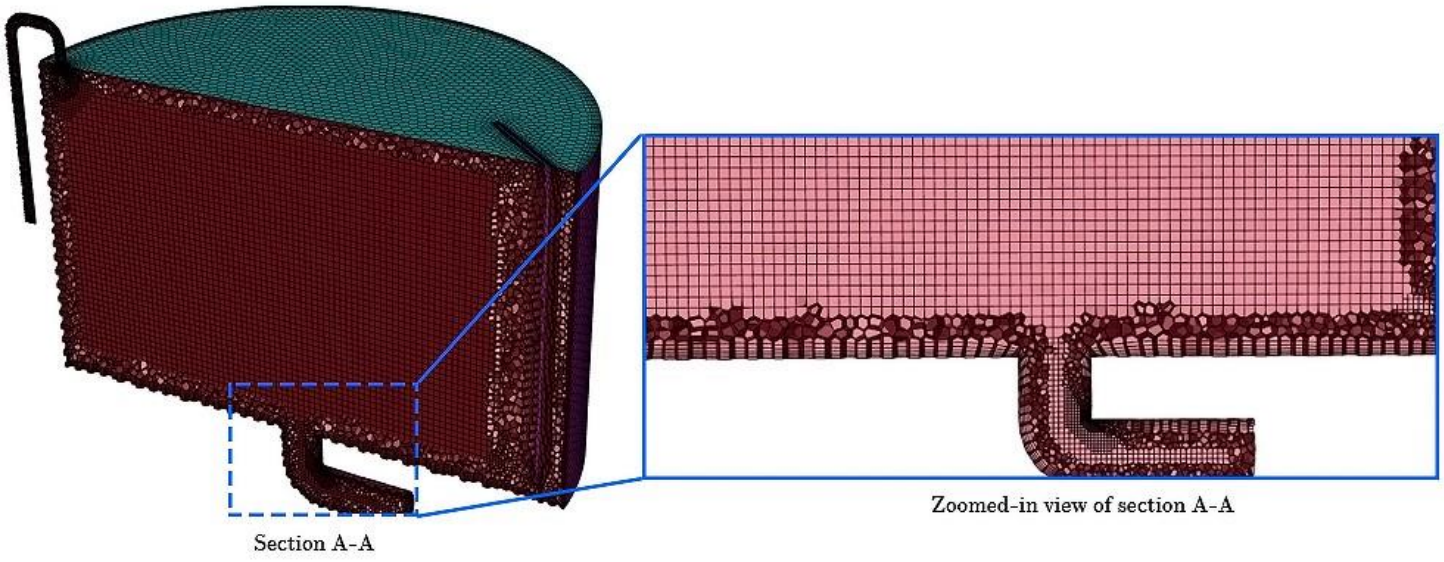

Figure 13. Mesh generated by ANSYS Fluent Meshing tool using Poly-hexcore method, in the zoomed-in section, different mesh elements could be seen, generated by this method

4.2 Setting Initial Conditions for The Solution

4.2.1 Boundary Conditions

For any fluid domain, boundary conditions define the inputs of a presented simulation model. Some of the conditions are pressure, velocity and volumetric flow rate. These conditions connect the simulation model with its surroundings. Without them, the simulation is not defined, and in most cases cannot proceed in finding a defined result. The boundary conditions set for this study are as the following:

- Inlet – (Mass flow rate)
- Outlet – (Pressure)
- Interior – (Solid)
- Symmetry – (Surface)
- Wall – (Solid stationary)
- Wall baffle – (Solid stationary)

As seen in Figure 11. A baffle is set in the tank model. The concept of the baffle was introduced to the geometrical model, for the purpose of decreasing the velocity flow of the fluid in the area situated behind the baffle. This decrease in velocity allows the fish being cultivated to rest, and lay eggs without being affected by the flow of the fluid, which influences the welfare of the cultivated fish and insures a higher growth rate. A contour representation of the velocity magnitude in three different horizontal planes; showing the effects of the baffle on the flow pattern and velocity magnitude of the fluid, could be seen below. This representation was calculated with 1000 iterations, for an inlet of volumetric flow rate 0.5 L/s.

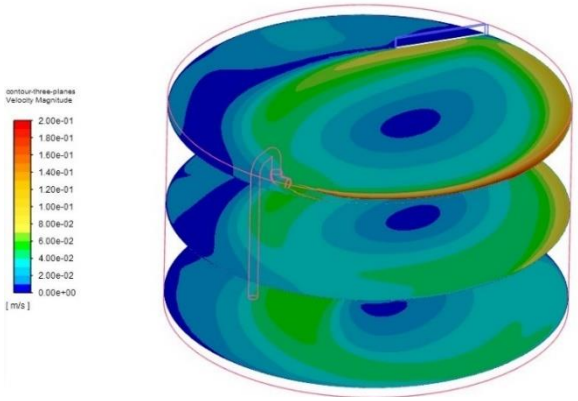

Figure 14. Contour representation of the baffle effects on the velocity magnitude in three different horizontal planes, for an inlet of volumetric flow rate 0.5 L/s, generated by ANSYS solver toolkit

4.2.2 **Turbulence models in RANS**

As mentioned previously, the vast majority of turbulent flow computations has been and for the foreseeable future will continue to be carried out with procedures based on the Reynolds-averaged Navier–Stokes (RANS). Despite that, the RANS model needs some additional equations to conclude a closed system. In order to be able to compute turbulent flows with the RANS equations, it is necessary to develop turbulence models to predict the Reynolds stresses and scalar transport terms, and close the system of mean flow equations. The most common RANS turbulence models are classified on the basis of the number of additional transport equations that need to be solved along with the RANS flow equations (Versteeg H. K. et al., 2007). Some of these models are:

- Spalart–Allmaras model
- k–ε model k: (turbulence kinetic energy), ε: (dissipation rate of turbulence kinetic energy)
- k–ω model k: (turbulence kinetic energy), ω: (the specific dissipation rate)

The Spalart-Allmaras model is a one-equation model, which is developed and used extensively for aerospace industrial applications. Whereas for elliptic flows, like recirculating and separated ones, experimental data is generally not available for the Spalart-Allmaras model, and its performance was found not to be superior, compared to the two-equation models.

The k–ε and k–ω models, are a two-equation based models, that are widely accepted and tested. The k–ε model is shown to be reliable for free-shear flows with small pressure gradients, but it may not be the best model for problems with large separations, adverse pressure gradients, or complex flows with strong curvatures. The k-epsilon is a model that predicts values far away from the boundaries (wall). As for the k–ω model, it can be used for low Reynolds number flows, with a relatively thick boundary layer, and a viscous sublayer that can be resolved. The k-omega model is best used for near-wall treatment (Argyropoulos C.D. et al., 2014).

As for the presented work, the model used is k–ω SST, where SST stands for (shear stress transport). The SST formulation switches to a k–ε behavior in the free-stream, which avoids the k−ω problem of being sensitive to the inlet free-stream turbulence properties, combining the best of both models.

4.2.3 **Coupling and Fluid Structure Interactions**

Fluid structure interactions are defined as when the flow around a body has a significant impact on the structure, and vice versa. Fluid dynamics and structural dynamics are two disciplines involved in these types of multiphysics problems, and they can both be described using continuum mechanics relations. Solution strategies for fluid structure interactions simulations are mainly divided into, monolithic and partitioned methods. These partitioned methods are divided into one-way and two-way coupling. For one-way coupling calculations, only the fluid pressure acting at the structure is transferred to the structure solver, whereas for two-way-coupling calculations, the displacement of the structure is also transferred to the fluid solver (Benra F. K. et al., 2011). In regards to this work, a one-way coupling method was used, which reduces the computational effort compared to the two-way coupling.

4.2.4 **Materials Used for The Simulation**

The material of the fluid domain that was used in the simulation was assumed to be water, of density $\rho = 998.2\ kg/m^3$ and kinematic viscosity $v = 1.004 \times 10^{-6} m^2/s$, where the particles entering the fluid domain considered to be of inert mass (not massless). Particles of different densities were introduced to the simulation, by the experiment that was provided and mentioned in Table 2 and 3. Where the TM0 pellet type has a density of $1054.4\ kg/m^3$,and $1072.9\ kg/m^3$ for the TM75 type.

4.3 Injections and Residence Time

Injections can be defined as a way of introducing particles of inert mass into a defined fluid domain. There are numerous methods of introducing injections. Some of the injection types that ANSYS fluent solver utilizes are the surface injection method, group injections method and single injection method. In our case, we have applied the group injections approach. This approach is used when it is necessary to define a range for one or more of the initial conditions, such as the range of initial positions or diameters of injection.

For this simulated experiment, a set of group injections with positions ranging from 0-8 as shown in Figure 15., where injected on the surface of the circular tank's fluid domain. Each injection contained 500 particles that represented the Rosin–Rammler size distribution parameters that was determined in the previous chapter. Points 1-8 were positioned on a circle with a radius of 2/5 of the tank's original radius R. The sphericity of the irregular particles as previously mentioned to be as $\phi = 0.874$. For this calculation the tank was in steady state, with an inlet of volumetric flow rate of 0.5 L/s.

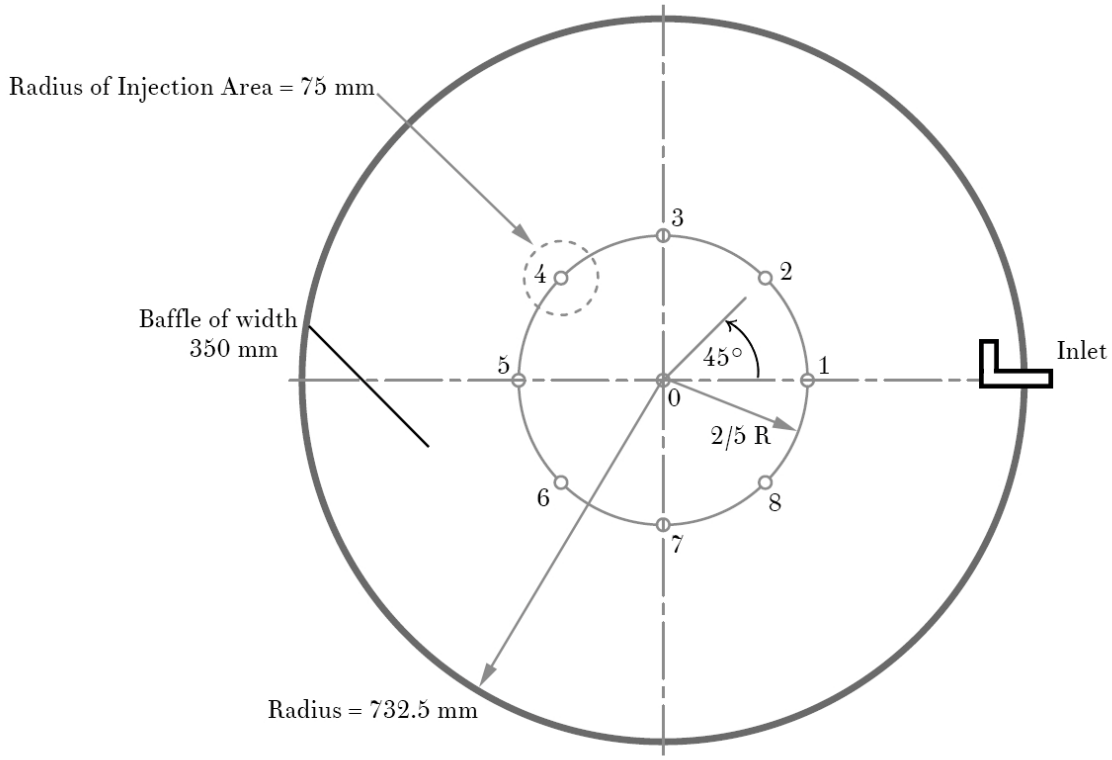

Figure 15. Positions 0-8 of the group injections applied on the circular tank's surface

The main goal of this experiment was to determine the mean residence time for all the injected positions used in the simulation, as shown in Figure 15. The mean residence time refers to the time it takes for a particle to escape the fluid domain from the injection position from which it was initially released. The results of the mean residence time for both type TM0 and TM75 pellets were generated by the help of ANSYS Particle Tracking, and could be represented graphically and numerally as shown below.

Table 5. Mean residence time of injected positions 0-8, for TM0 and TM75 feeding pellet types

Position	Angle [˚]	TM0 Mean Residence Time (s)	TM75 Mean Residence Time (s)
0	-	34.08	29.76
1	0	113.7	115.6
2	45	121.1	123.9
3	90	133.9	138.0
4	135	142.9	147.1
5	180	146.9	151.5
6	225	144.9	150.0
7	270	137.7	141.8
8	315	125.3	128.6

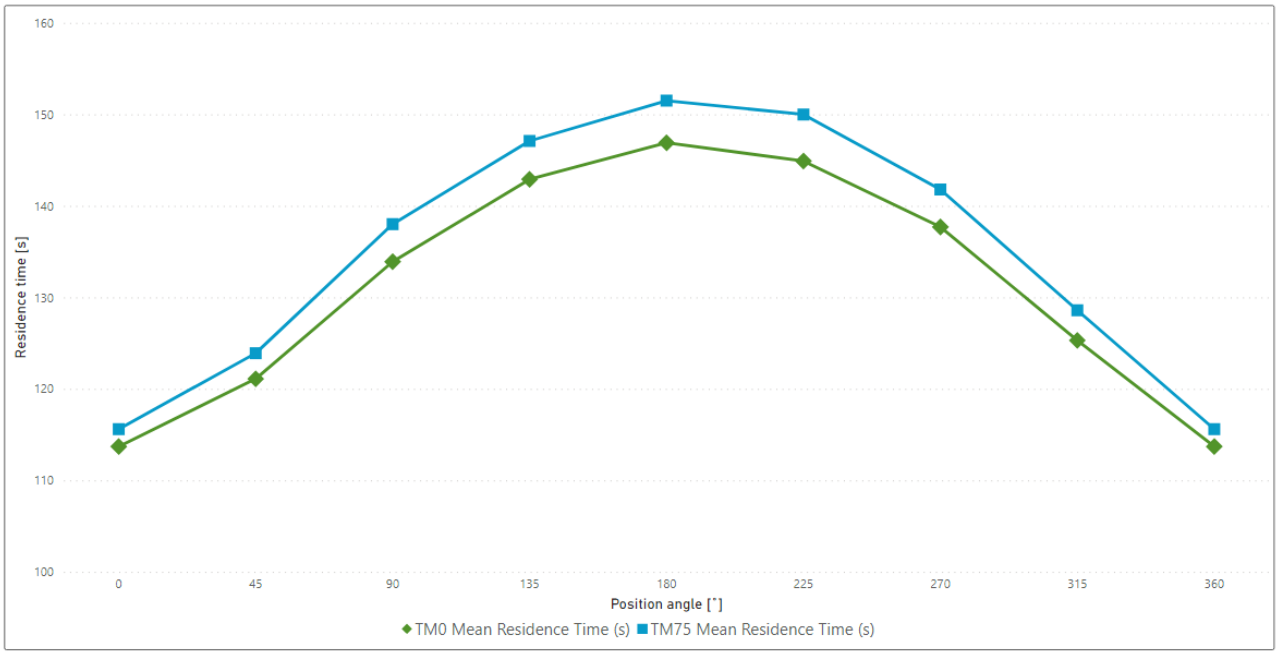

Figure 16. Graphical representation for the dependency of the mean residence time with respect to the position angle

The results presented above, clearly show that the largest mean residence time taken for both types of feeding pellets, obtained from the injection of particles in position 5, but this position wouldn't be characterized as an optimal position for feeding fish of all types. Where a variety of fish that can be cultivated in recirculating tanks exists, in which each fish type behaves differently while trying to eat. Some fish types swim and eat at a faster rate than other fish types that do so in a slower manner.

The concluded results for the mean residence time were calculated to be presented for marine biologists, and fish cultivating enthusiasts, where they would be able to categorize each fish type depending on the fish's movement and eating habits, with a favorable injection position for this specific tank and it's given properties.

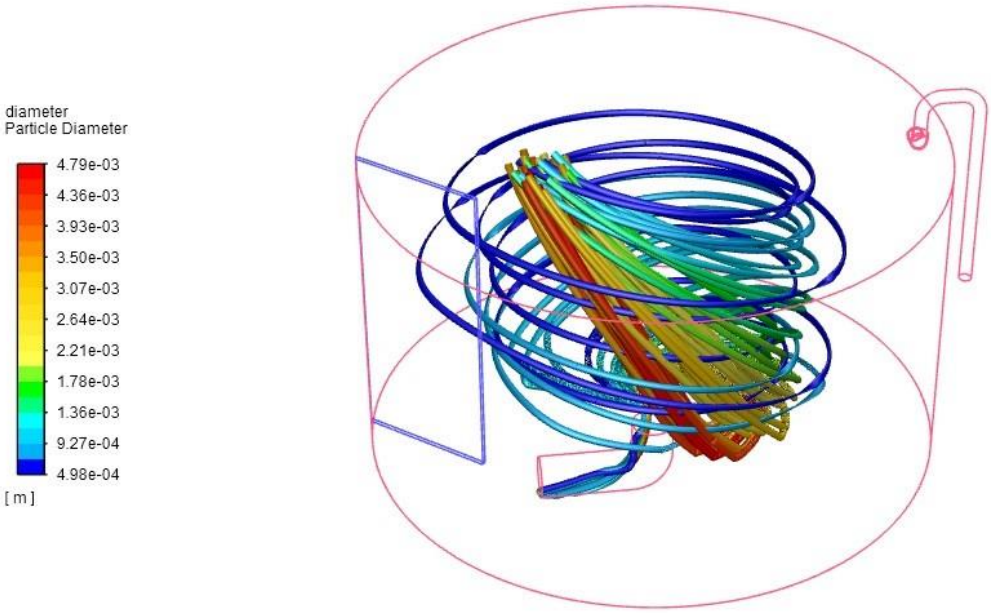

Figure 17. A graphical representation of TM75 pellets trajectory, released from the injection of position 5. Where the colors represent the pellet diameter according to the Rosin–Rammler size distribution method.

Conclusion

The purpose of this thesis was to create a computational fluid dynamics model for a cylindrical recirculating aquaculture system (using ANSYS fluent software), in order to evaluate the flow motion of feeding pellets, and assess its suitability for an aquatic environment.

Experimental data from sedimentation experiment were provided to deduce the effective density of the pellets, which was established on the basis of measuring the settling velocity of pellets in a water column. For further analysis the pellets' mean diameters was characterized by the Rosin–Rammler size distribution methodology.

The pellets were introduced to the simulated fish tank through injections of various positions for the purpose of evaluating the mean residence time of each injected position, where the residence mean time is to be considered as a crucial factor in designing fish cultivating tanks. The resulting evaluation of the mean residence time for each position concluded that the shortest time for both feeding pellet types, was positioned in the middle of the tank at position 0, and the longest residence mean time was evaluated at position 5 for both types. Compared to the previous study (Papáček Š. et al., 2020) the residence times are substantially larger, which is due to the baffle in the tank. Its position could be part of further optimizations with respect to self-cleaning capability of the system.

This presented computational fluid dynamics simulation might be of good use for marine biologists and fish farmers, who are interested in finding optimal positions for feeding and cultivating fish of different types.

Regarding future prospects in this field, the aim is to reduce the difference between the computational fluid simulation and the actual aquatic environment used nowadays. One proposal is to include the excrement characteristics for the fish type being farmed to the simulation as particles of inert mass, which would bring the simulation closer to a realistic environment. This might not affect the results drastically, but it always depends on types and sizes of the fish being cultivated.

A special mention to (Papáček Š. et al., 2020) which was the inspiration of the overall concept for this study, and to (Hanák J., 2016) which introduced the design and model of the simulated tank.

References

Almeida D. B. et al. (2021). Aquaculture. *Microbial community dynamics in a hatchery recirculating aquaculture system (RAS) of sole (Solea senegalensis), 593*, 736592.

ANSYS Inc. (2015). Mesh Quality and Advenced Topics Ansys Workbench. *ANSYS*, 1-37.

Argyropoulos C.D. et al. (2014). Recent advances on the numerical modelling of turbulent flows. *Applied Mathematical Modelling*, 693-732.

Benra F. K. et al. (2011). A Comparison of One-Way and Two-Way Coupling Methods for Numerical Analysis of Fluid-Structure Interactions. *Journal of Applied Mathematics*, 2-16.

Farghally H. M. et al. (2014). Control methodologies based on geothermal recirculating aquaculture system. *Energy*, 826-833.

Haider A. et al. (1989). Drag Coefficient and Terminal Velocity of Spherical and Nonspherical Particles. *Powder Technology,*, 63-70.

Hanák J. (2016). CFD simulation of flow in fish tanks. *Master Thesis, Czech Technical University in Prague*, 1-99.

Helfrich L. A. et al. (2013). Fish farming in recirculating aquaculture systems. *Department of Fisheries and Wildlife Sciences,Virginia Tech*, 1-19.

Li D. et al. (2017, August). Aquacultural Engineering. *Detection of uneaten fish food pellets in underwater images for aquaculture, 78*, 85-94.

Miardi. A. (2020). Experimental and CFD analysis of feed pellets in fish tank. *Bachelor thesis,Czech Technical University in Prague*, 1-38.

Morsi S. A. et al. (1972). An investigation of particle trajectories in two-phase flow systems. *Journal of Fluid Mechanics, 55*(2), 193-208.

Mosaic. (2018). ANSYS Fluent Mosaic Technology Automatically Combines Disparate Meshes. *ANSYS*, 1-8.

Papáček Š. et al. (2020). Experimental & Computational Fluid Dynamics Study of the Suitability of Different Solid Feed Pellets for Aquaculture Systems. *Applied Sciences*, 1-15.

Versteeg H. K. et al. (2007). *An Introduction to Computational Fluid Dynamics.* England: Pearson Education Limited.

Wadell H. A. (1934). Volume, Shape and Roundness of Rock Particles. *The Journal of Geology*, 443-451.

White F. M. (2007). *Viscous Fliud Flow.* New York: McGraw-Hill.

Yan S. et al. (2019). Drag coefficient prediction for non-spherical particles in dense gas–solid two-phase flow using artificial neural network. *Powder Technology*, 115-124.

Zhang Z. et al. (2007). Comparison of the Eulerian and Lagrangian methods for predicting particle transport in enclosed spaces. *Atmospheric Environment*, 5236-5248.